RSC Advances

PAPER

Check for updates

Cite this: *RSC Adv.*, 2019, **9**, 26894

Highly improved photocatalytic degradation of rhodamine B over $Bi_2Ga_{4-x}Fe_xO_9$ solid solutions under visible light irradiation†

Jia Yang,*[a] Xiaorui Sun,*[a] Chunmei Zeng,[b] Xiaoting Wang,[a] Yilan Hu,[a] Ting Zeng[a] and Jianwei Shi[a]

Received 20th June 2019
Accepted 13th August 2019

DOI: 10.1039/c9ra04632a

rsc.li/rsc-advances

In this work, $Bi_2Ga_{4-x}Fe_xO_9$ ($0 \leq x \leq 1.2$) solid solutions were prepared *via* the traditional high-temperature solid-state reaction. The Le Bail fitting on the powder X-ray diffraction patterns shows that these solid solutions were successfully synthesized. Scanning electron microscopy showed that the $Bi_2Ga_{3.2}Fe_{0.8}O_9$ sample was composed of sub-micron particle crystallites. Energy dispersive spectroscopy analysis and X-ray photoelectron spectroscopy were used to identify that the Fe element is trivalent when doping into the crystal structure. Ultraviolet-visible diffused reflectance spectra suggested that the bandgap of $Bi_2Ga_{3.2}Fe_{0.8}O_9$ is narrower than that of the undoped $Bi_2Ga_4O_9$ sample. Three strategies, including Fe^{3+} doping, addition of H_2O_2, and loading of the cocatalyst, were utilized to improve the photocatalytic degradation activity. The optimum photocatalytic performance was obtained over 2.5 wt% Cu/$Bi_2Ga_{3.2}Fe_{0.8}O_9$ sample in 20 ppm RhB aqueous solution (containing 1.5 mL H_2O_2) under visible light irradiation. Its photodegradation rate is 8.0 times that of $Bi_2Ga_4O_9$ containing 0.5 mL H_2O_2. The 2.5 wt% Cu/$Bi_2Ga_{3.2}Fe_{0.8}O_9$ photocatalyst remained stable and active even after four cycles. Also, its photocatalytic conversion efficiency for RhB was nearly 100%, which was achieved in 3 hours. The photocatalytic mechanism indicated that ·OH and h^+ played an important role in the photocatalytic degradation reaction.

1. Introduction

Dye effluents from textile industries and photographic industries are becoming a serious environmental problem because of their toxicity, unacceptable color, high chemical oxygen demand, and biological degradation.[1–3] Many advanced oxidation technologies, especially photocatalytic technology, were developed to treat industrial wastewater.[4] Photocatalysis is a green technique for the degradation of various dyes such as rhodamine B (RhB), brilliant blue, thionine, and methylene orange.[5–8] The most important point is that the semiconducting material, such as single semiconductor, semiconducting heterostructure, or solid solution, was utilized as the photocatalyst in this type of reaction.[9–14] However, a majority of semiconductors, such as TiO_2, $Ca_2PbGa_8O_{15}$, and ZnO, only have a response under ultraviolet light irradiation.[15–17] The ultraviolet spectrum and visible spectrum account for 4% and 46% of the solar spectrum, respectively.[18] Hence, discovering a new photocatalyst for the photocatalytic degradation reaction is an event of significance.

Usually, the Bi-based oxides have sensitive activity under visible light. The famous $BiVO_4$ material was extensively studied for visible-light photocatalytic applications such as oxygen evolution, water splitting, carbon dioxide reduction, and dye degradation.[19–22] The other Bi-based oxides, such as Bi_2O_3, Bi_2MoO_6, Bi_2WO_6, $BiTaO_4$, $PbBi_2Nb_2O_9$, and $CdBiYO_4$, were studied as visible-light-driven photocatalysts for photocatalytic applications as well.[23–28] The visible-light response of these materials arises due to the presence of the Bi^{3+} lone pair of electrons. It was found that the bandgap shrinking was due to the contribution of Bi 6s orbitals to the valence band composition. However, the conduction bands of these Bi-based oxide compounds are more positive than 0 V, which means that they cannot be used for hydrogen evolution by themselves. Recently, $Bi_2Ga_4O_9$ was employed as the photocatalyst for water splitting under visible-light irradiation.[29] Therefore, it is interesting to investigate the visible-light photocatalytic degradation performance of $Bi_2Ga_4O_9$.

To the best of our knowledge, there has been no report regarding the application of $Bi_2Ga_4O_9$ in the visible-light driven degradation of dyes. Herein, the photocatalytic degradation performance of mullite type $Bi_2Ga_4O_9$ was improved by doping Fe^{3+} ions, adding H_2O_2, and loading cocatalysts (such as Cu, Ag,

[a]*Chongqing Key Laboratory of Inorganic Special Functional Materials, College of Chemistry and Chemical Engineering, Yangtze Normal University, Fuling, Chongqing 408100, P. R. China. E-mail: sunxiaoruiyznu@163.com; yangjiayznu@163.com; Tel: +86-18883876787; +86-18716372096*

[b]*Chemical Synthesis and Pollution Control Key Laboratory of Sichuan Province, College of Chemistry and Chemical Engineering, China West Normal University, Nanchong 637002, P. R. China*

† Electronic supplementary information (ESI) available. See DOI: 10.1039/c9ra04632a

Au, Pt, Ni, and Ru). RhB was used as the model organic dye to study the photocatalytic property of the as-prepared samples. In particular, the composition, morphology, physical property, and photocatalytic mechanism of $Bi_2Ga_{3.2}Fe_{0.8}O_9$ were systematically investigated.

2. Materials and methods

2.1 Preparation of the catalysts

The solid-state method was applied to synthesize $Bi_2Ga_{4-x}Fe_xO_9$ ($0 \leq x \leq 1.2$) samples. The starting materials, Bi_2O_3 (99.9%, Sinopharm Chemical Reagent Co., Ltd.), Ga_2O_3 (99.99%, Alfa Aesar), and Fe_2O_3 (99.5%, Sinopharm Chemical Reagent Co., Ltd.), were used after pre-calcination at 600 °C to remove the possible absorbed moisture or CO_2. Typically, for the synthesis of $Bi_2Ga_{3.2}Fe_{0.8}O_9$, stoichiometric amounts of the reagents were homogenized using an agate mortar, followed by preheating at 600 °C for 10 h. The resultant powder was manually re-ground thoroughly. Finally, it was heated at 850 °C for another 15 h in air.

2.2 Preparation of the cocatalysts

The metal cocatalyst was loaded on $Bi_2Ga_{3.2}Fe_{0.8}O_9$ by a photodeposition method.[29] For instance, 100 mg $Bi_2Ga_{3.2}Fe_{0.8}O_9$ sample together with 7.8 mL of $CuCl_2$ (0.32 mg mL^{-1}) was mixed in 200 mL 2 vol% methanol aqueous solution. This solution, in a 300 mL Pyrex glass reactor, was stirred for 10 minutes and then the mixture was irradiated by a 300 W high-pressure Hg-lamp (CEL-LAM300, Beijing AuLight Ltd. Co., intensity of light is 49.5 mW cm^{-2}) for 1 hour. After this, the sample was washed with distilled water and dried to be used as a photocatalyst. This sample was denoted as 2.5 wt% Cu/$Bi_2Ga_{3.2}Fe_{0.8}O_9$.

2.3 Characterization

The crystal structure of the as-prepared sample was characterized by X-ray diffraction (XRD, XRD-6100AS, Cu Kα irradiation, Shimadzu, Japan). Le Bail refinements were performed to obtain the cell parameters using TOPAS software package. The morphology and size of the samples were characterized by scanning electron microscopy (SEM FEI verios 460) equipped with an energy dispersive spectrometer (EDS). The compositions of the $Bi_2Ga_{3.2}Fe_{0.8}O_9$ sample were analyzed with inductively coupled plasma-atomic emission spectroscopy (ICP-OES, PerkinElmer 8300). X-ray photoelectron spectroscopy (XPS) was carried out using a PHI5000 spectrometer with an Al Kα (15 kV) X-ray source. Ultraviolet-visible diffused reflectance spectra (DRS) were obtained on a Shimadzu UV-3600 spectrometer equipped with an integrating sphere attachment. The analysis range was from 200 to 1100 nm and $BaSO_4$ was used as the reflectance standard. The number of incident photons was measured by using a calibrated Si photodiode (CEL-NP2000).

2.4 Photocatalytic performance evaluation

The photocatalytic performance was tested on the reaction equipment, which contains a 300 mL Pyrex glass reactor and a quartz cold trap. In a typical run, 100 mg of the catalyst was dispersed by a magnetic stirrer in 250 mL of 20 ppm RhB aqueous solution. The solution was continuously stirred and a self-made circulating cooling water system maintained the temperature of the reaction system at 25 ± 5 °C. The light irradiation source was generated by an external 300 W long-arc xenon lamp (CEL-LAX300, Beijing AuLight Ltd. Co., intensity of light is 38.5 mW cm^{-2}).

These photocatalysts with 250 mL Rh (20 ppm) solution were stirred in dark for 30 min to achieve the adsorption–desorption equilibrium. After light illumination at regular time intervals, the concentration of the RhB solution was monitored with a Shimadzu UV2600 UV-Vis spectrophotometer at 10 minute intervals.

2.5 Determination of the reactive species

The photocatalytic mechanism of 2.5 wt% Cu/$Bi_2Ga_{3.2}Fe_{0.8}O_9$ was studied in accordance with part 2.4, but before the start of the reaction, some quenchers (1 mmol L^{-1}) were added into the RhB solution, such as *p*-benzoquinone (BQ; $\cdot O_2^-$ radical scavenger), disodium ethylenediaminetetraacetate (EDTA-2Na; h^+ scavenger), and isopropanol (IPA; ·OH radical scavenger).

3. Results and discussion

Fig. 1 presents the XRD patterns of $Bi_2Ga_{4-x}Fe_xO_9$ ($0 < x < 1.2$) solid solutions and the sharp peaks indicate the high crystallinity of these samples. Compared to the simulated XRD pattern (ICSD-250413) of $Bi_2Ga_4O_9$, it is evident that the pure phases of the $Bi_2Ga_{4-x}Fe_xO_9$ ($0 \leq x \leq 1.2$) solid solutions were synthesized without any impurity peak. As shown in the inserted red rectangle of Fig. 1, we selected the section of 2θ from 28° to 29.5° to observe the peak shift by Fe^{3+}-doping. The peaks of the solid solutions shifted linearly to a smaller angle. This means that the Fe^{3+} ions were incorporated successfully into the crystal structure of $Bi_2Ga_4O_9$.[30] We can determine the change in the cell lattice parameters (*a*, *b*, *c*, and *V*) by Le Bail fitting of the whole

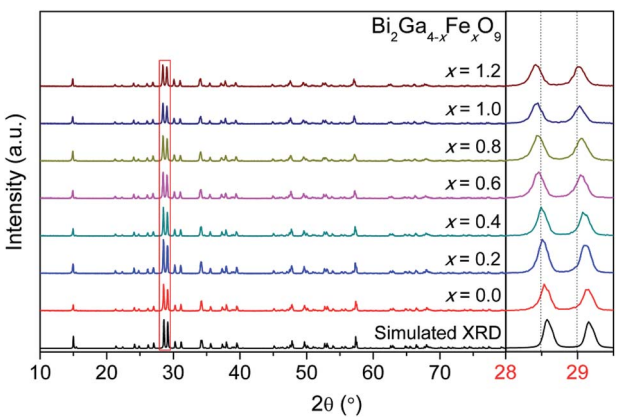

Fig. 1 The powder XRD patterns for the solid solutions, where the simulated XRD pattern for the un-doped $Bi_2Ga_4O_9$ is also given at the bottom. Also, the inserted red rectangle was magnified to the right of the XRD patterns.

XRD patterns. The plot of the crystallographic data for a, b, c, and V along with an increase in x suggests a linear swell (see Fig. S1†).[31] The crystal structure of $Bi_2Ga_{3.2}Fe_{0.8}O_9$ can be confirmed by TOPAS (see Fig. S2†). These results strongly suggest that Fe^{3+} has been successfully doped into $Bi_2Ga_4O_9$ without any structural change.

The as-prepared $Bi_2Ga_4O_9$ and $Bi_2Ga_{3.2}Fe_{0.8}O_9$ were observed by electron microscopy. The SEM images of the $Bi_2Ga_{3.2}Fe_{0.8}O_9$ powders were composed of uneven sized particles in the range of 0.4–1 μm (see Fig. 2). The particle size of the $Bi_2Ga_{3.2}Fe_{0.8}O_9$ powder was remarkably smaller than that of the undoped $Bi_2Ga_4O_9$ powder, which is in the range of 0.8–1.5 μm (see Fig. S3†). Both the particles were well-crystallized, which is consistent with the XRD analysis. Elemental analysis was performed on the $Bi_2Ga_{3.2}Fe_{0.8}O_9$ sample, which gave an average atomic ratio of Bi : Ga : Fe : O = 2.00 : 3.35 : 0.83 : 9.18 (see Fig. S4†). Also, this sample was analyzed by ICP, which gave a close metallic atomic ratio of Bi : Ga : Fe = 2 : 3.27 : 0.73. Besides, the XPS spectra for $Bi_2Ga_{3.2}Fe_{0.8}O_9$ indicated that not only the elemental compositions are in agreement with the EDS result but also support the fact that the Fe element is trivalent (see Fig. S5†).

Fig. 3 shows the DRS of the $Bi_2Ga_4O_9$ and $Bi_2Ga_{3.2}Fe_{0.8}O_9$ samples. The spectrum of $Bi_2Ga_4O_9$ showed a typical bandgap transition similar to the other semiconductors, such as C_3N_4 and $CuFeS_2$.[32,33] The spectrum of $Bi_2Ga_{3.2}Fe_{0.8}O_9$ showed an obvious red shift and enhancement in comparison to the spectrum of $Bi_2Ga_4O_9$ (see Fig. 3a). There is an absorption peak in the range of 625–750 nm, which is due to the d–d transition of the Fe^{3+} ion.[29] For most semiconductors, the bandgap energy E_g can be calculated by the following equation: $\alpha h\nu = A(h\nu - E_g)^{n/2}$, where h, ν, and A are the Planck's constant, light frequency, and proportionality, respectively; n is determined on the basis of the transition type (*i.e.*, $n = 1$ for direct transition, $n = 4$ for indirect transition).[13] The best fit of $(\alpha h\nu)^2$ *vs.* E_g was obtained only when n is 1, suggesting that direct transitions across the energy bandgaps of $Bi_2Ga_4O_9$ and $Bi_2Ga_{3.2}Fe_{0.8}O_9$ are allowed (see Fig. 3b). The extrapolated value of $h\nu$ at $\alpha = 0$ gives an absorption edge energy corresponding to E_g, which are 2.99 eV and 2.59 eV for $Bi_2Ga_4O_9$ and $Bi_2Ga_{3.2}Fe_{0.8}O_9$, respectively. Besides, on comparing the absorption spectra of $Bi_2Ga_{4-x}Fe_xO_9$ with different Fe contents ($0 < x < 1.2$), the absorption edge appeared to show a "red shift" with increasing Fe^{3+} concentration (see Fig. S6†).

The photocatalytic activities were evaluated for the $Bi_2Ga_{4-x}Fe_xO_9$ ($0 < x < 1.2$) samples using the catalytic degradation of RhB as a probe reaction under visible light irradiation. The absorption–desorption equilibrium was established by stirring the reaction solution mixed with the photocatalyst powder in

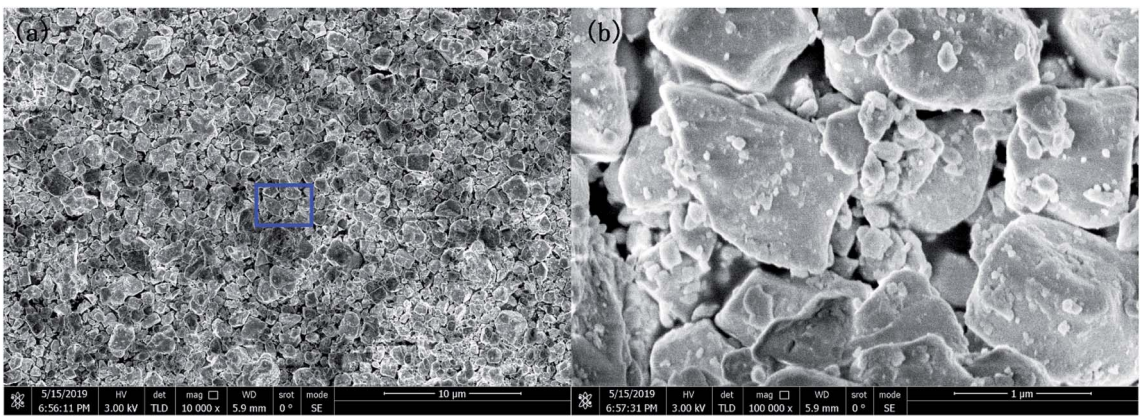

Fig. 2 SEM images for $Bi_2Ga_{3.2}Fe_{0.8}O_9$.

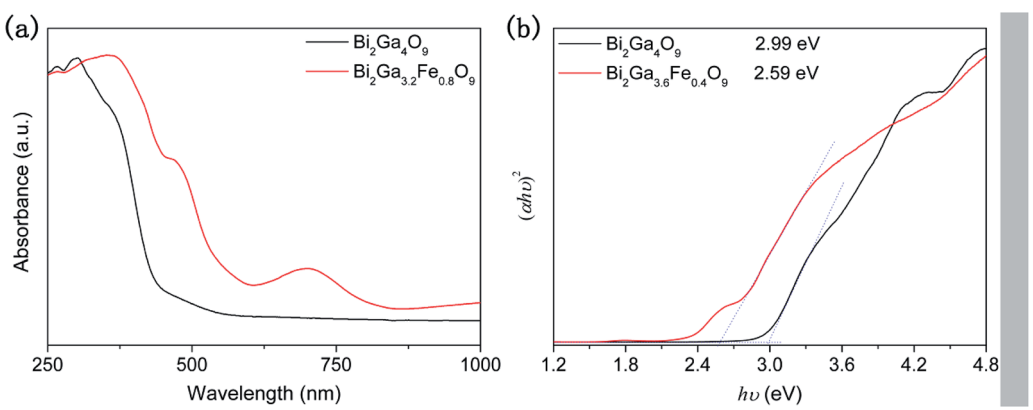

Fig. 3 (a) UV-Vis diffused reflectance spectrum for $Bi_2Ga_4O_9$ and $Bi_2Ga_{3.2}Fe_{0.8}O_9$. (b) The estimated bandgap energy E_g with a plot of $(\alpha h\nu)^2$ against the photon energy ($h\nu$).

a darkroom for 30 min before illumination. Fig. 4 displays the results for RhB degradation using the $Bi_2Ga_{4-x}Fe_xO_9$ ($0 < x < 1.2$) samples under the same reaction conditions. As shown in Fig. 4a, the absorbance of the RhB reaction solution decreased rapidly after the visible light irradiation. To quantitatively assess the photocatalytic performance of the solid solutions, the reaction kinetics of RhB degradation were calculated by the first-order model with the $\ln(C_0/C)$ *versus* time plot (see Fig. 4b).[34] The calculated k values of $Bi_2Ga_{4-x}Fe_xO_9$, where $x = 0$, 0.2, 0.4, 0.6, 0.8, 1.0, and 1.2, are 0.0022 min^{-1}, 0.0026 min^{-1}, 0.0030 min^{-1}, 0.0053 min^{-1}, 0.0091 min^{-1}, 0.0082 min^{-1}, and 0.0060 min^{-1}, respectively. The k value of $Bi_2Ga_{3.2}Fe_{0.8}O_9$ is 4.1 times larger than that of the undoped $Bi_2Ga_4O_9$. Also, the kinetic constant for RhB degradation catalyzed by the undoped sample is the smallest. The conversion efficiency of the solid solutions displayed that the photocatalytic activity of $Bi_2Ga_{3.2}Fe_{0.8}O_9$ is better than that of the undoped $Bi_2Ga_4O_9$ as well (see Fig. 4c). The above results illustrate that doping a slight amount of Fe^{3+} into the $Bi_2Ga_4O_9$ crystal structure not only makes the photocatalyst economical but also significantly promotes the photocatalytic performance.[35] However, an excessive amount of Fe^{3+} plays the role of a recombination center for photogenerated electrons and holes.[18,36] Owing to the two effects, the optimum Fe^{3+} amount was 20 wt%; hence, the $Bi_2Ga_{3.2}Fe_{0.8}O_9$ sample exhibits the highest photocatalytic performance among the solid solutions. Fig. 4d displays that RhB was photocatalytically oxidized in one hour using the $Bi_2Ga_{3.2}Fe_{0.8}O_9$ sample.

Fig. 5 presents the conversion efficiency of RhB over the $Bi_2Ga_{3.2}Fe_{0.8}O_9$ sample under visible light irradiation. Usually, H_2O_2 plays a key role in the degradation of various dyes.[37,38] In this work, using the above optimum $Bi_2Ga_{3.2}Fe_{0.8}O_9$ sample without H_2O_2 displayed a very low conversion efficiency of RhB in the photocatalytic reaction. The conversion efficiency of RhB was significantly improved on increasing the usage amount of H_2O_2 by comparing the photocatalytic activity of $Bi_2Ga_{3.2}Fe_{0.8}O_9$ with 0 mL H_2O_2 (see Fig. 5a). Since excess H_2O_2 acts as a scavenger of ·OH and exhausts ·OH in the solution, an optimum amount of H_2O_2 is used.[39] The optimum k value of $Bi_2Ga_{3.2}Fe_{0.8}O_9$ with 1.5 mL H_2O_2 is 0.0108 min^{-1} (see Fig. S7†). Besides, the photodecomposition activity for RhB using only 1.5 mL H_2O_2 is better (see Fig. S8†). Six kinds of cocatalysts were loaded on the $Bi_2Ga_{3.2}Fe_{0.8}O_9$ sample to improve its photocatalytic performance. Generally, the metal cocatalyst played the role of an active site, which is beneficial for the separation of photogenerated electrons and holes.[40,41] However, only the Cu and Ag cocatalysts have a positive influence on the photocatalytic activity in our experiment (see Fig. 5b). Also, the optimum k value of $Bi_2Ga_{3.2}Fe_{0.8}O_9$ with 1 wt% Cu cocatalyst is

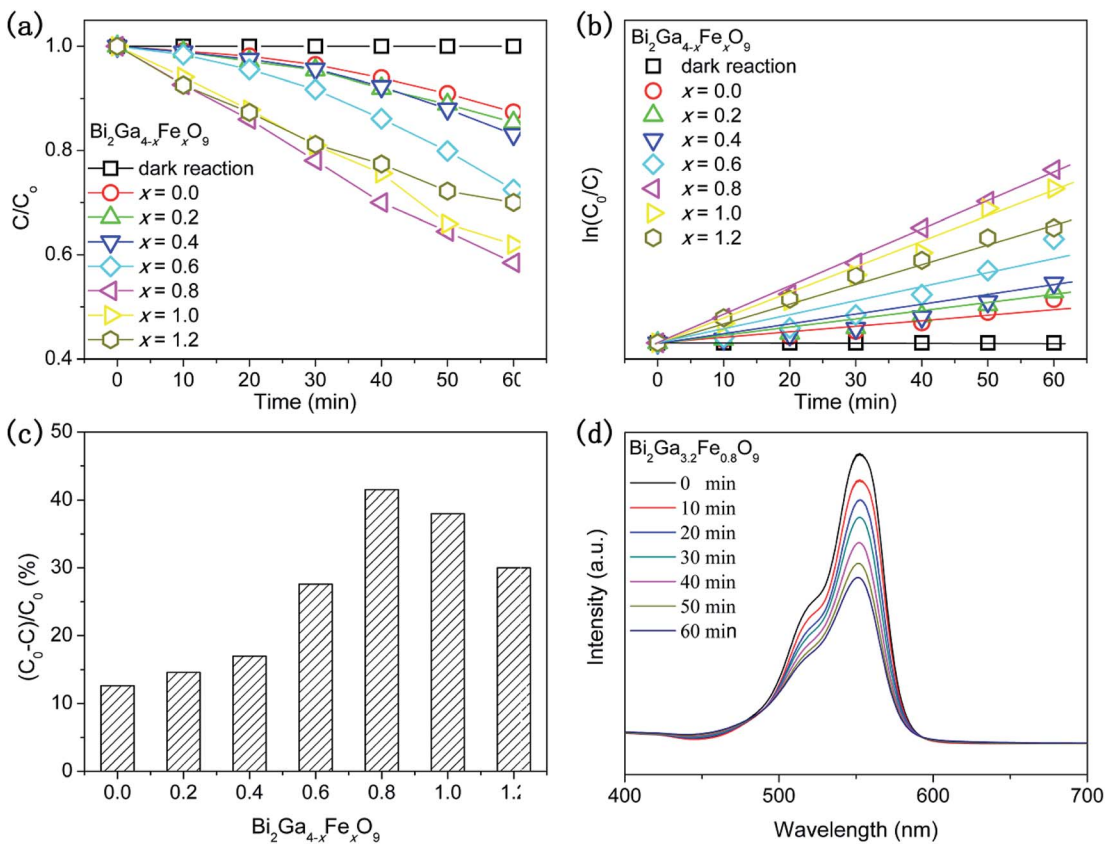

Fig. 4 (a) Photocatalytic degradation of RhB using $Bi_2Ga_{4-x}Fe_xO_9$ solid solutions under visible light irradiation. (b) First-order kinetic constants for the degradation of RhB under visible light irradiation. (c) The conversion efficiency of RhB over the solid solutions under visible light irradiation. (d) The UV-Vis absorption spectra of RhB at different concentrations using $Bi_2Ga_{3.2}Fe_{0.8}O_9$ as the photocatalyst under visible light irradiation. Photocatalytic conditions: 100 mg photocatalyst, 250 mL solution, RhB 20 ppm, pH = 6, $V(H_2O_2) = 0.5$ mL, 300 W long-arc xenon lamp.

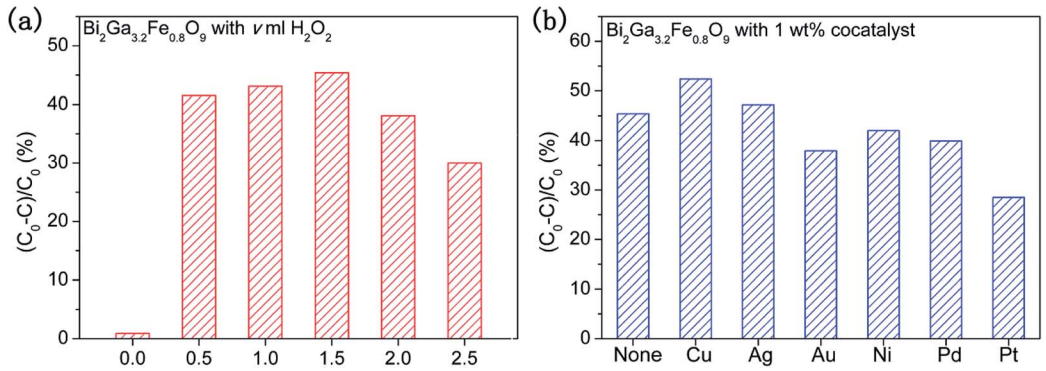

Fig. 5 The conversion efficiency of RhB over the $Bi_2Ga_{3.2}Fe_{0.8}O_9$ sample under visible light irradiation: (a) addition of different volumes of H_2O_2 in 250 mL solution; (b) loading 1 wt% of different cocatalysts on the photocatalyst. Photocatalytic conditions: 100 mg photocatalyst, 250 mL solution, RhB 20 ppm, pH = 6, 300 W long-arc xenon lamp.

0.0131 min^{-1} (see Fig. S9†). The possible reason will be discussed in the photocatalytic mechanism section.

The usage amount of Cu cocatalyst was tested for the photocatalytic degradation of RhB under visible light. The 2.5 wt% $Cu/Bi_2Ga_{3.2}Fe_{0.8}O_9$ displays the optimum photocatalytic activity (see Fig. 6a). Also, the corresponding optimum k value is 0.0175 min^{-1} (see Fig. S10†). The negative effect of excessive Cu may be caused by the interfacial charge recombination.[42] Other than photocatalytic efficiency, the stability and reusability of the photocatalyst is also an important factor to evaluate the property of the catalyst.[43] Therefore, the stability of the best performing 2.5 wt% $Cu/Bi_2Ga_{3.2}Fe_{0.8}O_9$ sample by photocatalytic degradation of RhB for four cycles under the same conditions was studied. Specifically, each cycle consisted of 60 min of photocatalytic reaction, followed by the separation of the photocatalyst by centrifugation, then washing with distilled water,

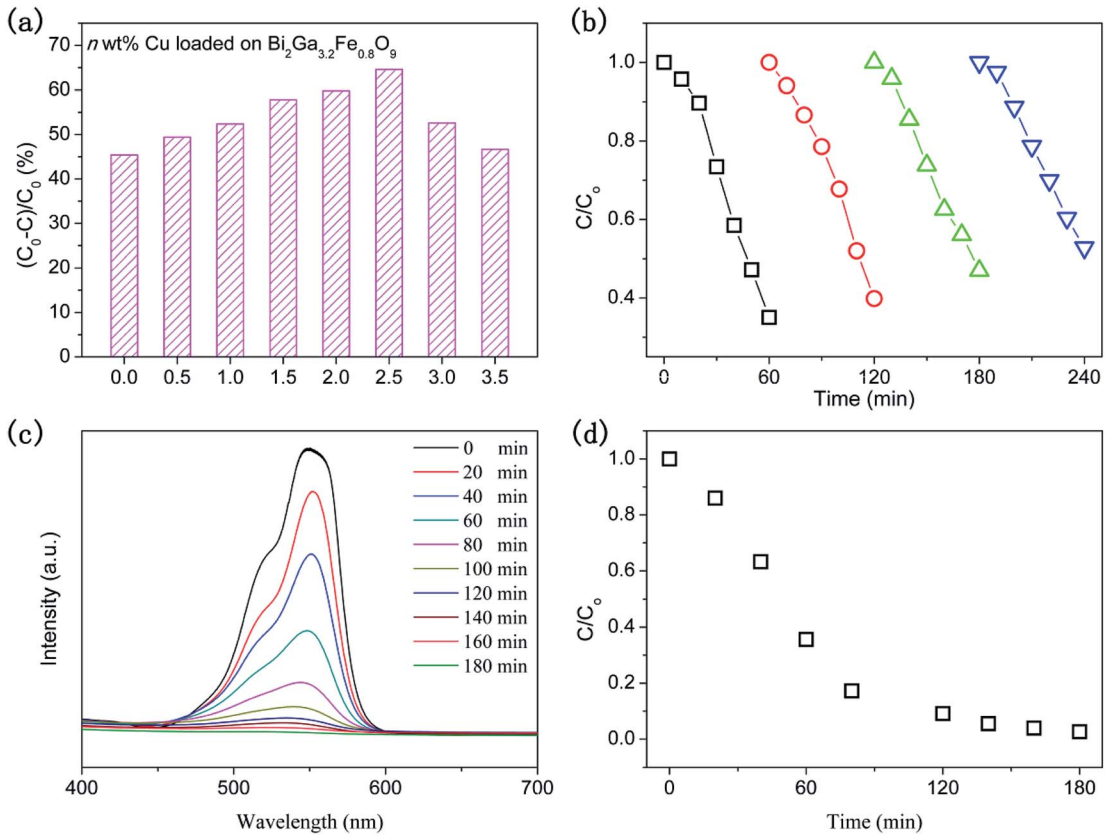

Fig. 6 (a) The conversion efficiency of RhB using $Bi_2Ga_{3.2}Fe_{0.8}O_9$ with different amounts of Cu-cocatalyst under visible light irradiation. (b) Cyclic photocatalytic degradation of RhB using 2.5 wt% $Cu/Bi_2Ga_{3.2}Fe_{0.8}O_9$ under visible light irradiation. (c) The UV-Vis absorption spectra of RhB with different concentrations using 2.5 wt% $Cu/Bi_2Ga_{3.2}Fe_{0.8}O_9$ as the photocatalyst under visible light irradiation. (d) Photocatalytic degradation of RhB using 0.5 wt% $Cu/Bi_2Ga_{3.2}Fe_{0.8}O_9$ under visible light irradiation. Photocatalytic conditions: 100 mg photocatalyst, 250 mL solution, RhB 20 ppm, pH = 6, $V(H_2O_2)$ = 1.5 mL, 300 W long-arc xenon lamp.

and finally drying of the photocatalyst in an oven at 60 °C. The change in the normalized concentration of RhB (C/C_0) over four cycles is displayed in Fig. 6b. The photocatalytic conversion efficiency of 2.5 wt% Cu/$Bi_2Ga_{3.2}Fe_{0.8}O_9$ sample decreased slightly after each cycle, such that 65% and 50% of RhB was degraded after the first and fourth cycles, respectively. The reduction in the photocatalytic activity is attributable to the inevitable loss of the photocatalyst during the separation and cleaning steps.[6] This demonstrates that the sample is relatively photo-stable in the photocatalytic reaction. Also, the XRD patterns of the photocatalysts after the photocatalytic reaction display the photo-stability of these samples (see Fig. S11†). Fig. 6c and d display that nearly 100% RhB was completely degraded in 3 hours.

The photocatalytic mechanism for the 1.5 wt% Cu/$Bi_2Ga_{3.2}Fe_{0.8}O_9$ sample was tested. We employ electronegativity to estimate the energy potential of the conduction band (CB) and valence band (VB) semi-quantitatively. The applied equations are $E_{VB} = \chi - E_e + 1/2E_g$ and $E_{CB} = E_{VB} - E_g$, where, χ is the Mulliken electronegativity; E_e is the energy of free electrons on the hydrogen scale, which is 4.50 eV.[29] E_g is the observed bandgap energy for $Bi_2Ga_4O_9$ and $Bi_2Ga_{3.2}Fe_{0.8}O_9$, which are 2.99 eV and 2.59 eV from DRS, respectively. χ for $Bi_2Ga_4O_9$ and $Bi_2Ga_{3.2}Fe_{0.8}O_9$ can be calculated by their molecular formulas, which were found to be 5.63 eV and 5.70 eV, respectively. So, the E_{CB} and E_{VB} of $Bi_2Ga_4O_9$ are −0.37 V and 2.62 V, respectively. The E_{CB} and E_{VB} of $Bi_2Ga_{3.2}Fe_{0.8}O_9$ are −0.09 V and 2.50 V, respectively. It can be clearly seen that the bandgap of $Bi_2Ga_{3.2}Fe_{0.8}O_9$ is narrower than that of $Bi_2Ga_4O_9$, and the absolute values of the CB and VB potentials for $Bi_2Ga_{3.2}Fe_{0.8}O_9$ are smaller than those of $Bi_2Ga_4O_9$. This shows that the photocatalytic activity of $Bi_2Ga_{3.2}Fe_{0.8}O_9$ is better than that of $Bi_2Ga_4O_9$. As we know, the photocatalytic active species, including h^+, ·OH, and $\cdot O_2^-$, play a very important role in the photocatalytic degradation reaction.[44,45] Therefore, the relative redox potentials of $O_2/\cdot O_2^-$, $OH^-/\cdot OH$, and $H_2O/\cdot OH$ are displayed in Fig. 7a.[43] We can conclude that $\cdot O_2^-$ has a slight influence over the $Bi_2Ga_{3.2}Fe_{0.8}O_9$ sample in the photocatalytic reaction. EDTA-2Na, IPA, and BQ were used as the quenchers for h^+, ·OH, and $\cdot O_2^-$, respectively (see Fig. 7b). It can be seen that the photocatalytic performance was slightly affected by adding BQ and the photo-degradation rate was 50.6%, indicating that $\cdot O_2^-$ played a small role in the photocatalytic degradation reaction. In contrast, compared with that without a quencher (64.6%), the photo-degradation rate reduced to 18.7% and 7.3%, respectively, which demonstrated that ·OH and h^+ played an important role in the photocatalytic degradation reaction. All the relevant reactions are described as follows:

$$Bi_2Ga_{3.2}Fe_{0.8}O_9 + h\nu \rightarrow Bi_2Ga_{3.2}Fe_{0.8}O_9(e^- + h^+)$$

$$e^-(Bi_2Ga_{3.2}Fe_{0.8}O_9) + H^+ \rightarrow 1/2H_2$$

$$h^+(Bi_2Ga_{3.2}Fe_{0.8}O_9) + OH^- \rightarrow \cdot OH$$

$$h^+(Bi_2Ga_{3.2}Fe_{0.8}O_9) + H_2O \rightarrow \cdot OH + H^+$$

$$Fe^{3+} + e^-(Bi_2Ga_{3.2}Fe_{0.8}O_9) \rightarrow Fe^{2+}$$

$$Fe^{2+} + H_2O_2 \rightarrow Fe^{3+} + \cdot OH + OH^-$$

$$H_2O \rightarrow H^+ + OH^-$$

$$\cdot OH + RhB \rightarrow \text{product}$$

$$h^+(Bi_2Ga_{3.2}Fe_{0.8}O_9) + RhB \rightarrow \text{product}$$

These processes can be used to explain the improvement in the photocatalytic activity of $Bi_2Ga_{3.2}Fe_{0.8}O_9$ using Cu and Ag. The active species other than the $\cdot O_2^-$ play an important role in the photocatalytic degradation reaction. This means that the photo-generated electron plays a small role in the photocatalytic reaction. Owing to the presence of methanol in the photo-deposition process, these cocatalysts mainly tend to be metals on the surface of the photocatalyst. As we know, the introduced metal mostly functions as the electron acceptor to manifest electron accumulation at the metal and hole localization at the semiconductor.[46,47] Besides, the cocatalyst has an influence on the reduction of the chemical barrier. Hence, with the assistance of the cocatalyst, the photo-generated electron was used to form H_2 and even $\cdot O_2^-$. However, RhB is a cationic dye, which is not easily absorbed on the surface of the photocatalyst.

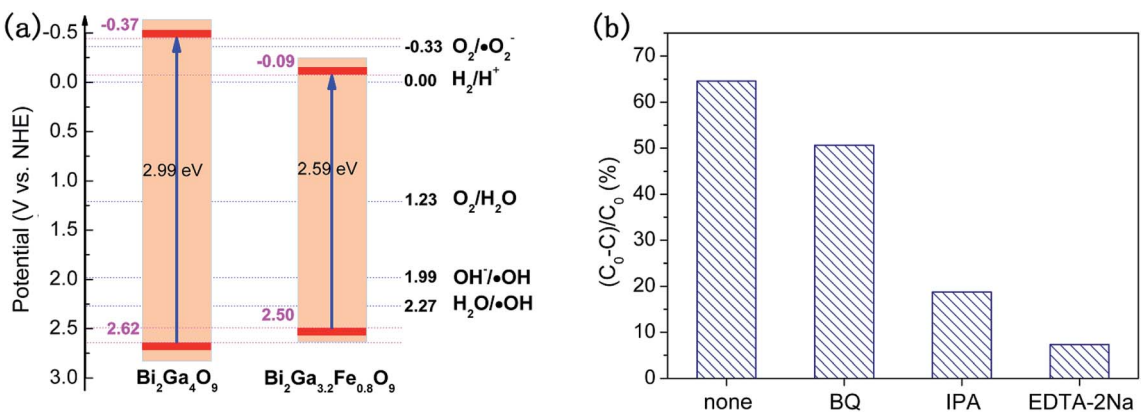

Fig. 7 (a) Schematic illustration of the band structure diagram of $Bi_2Ga_4O_9$ and $Bi_2Ga_{3.2}Fe_{0.8}O_9$. (b) The photocatalytic conversion efficiency of 2.5 wt% Cu/$Bi_2Ga_{3.2}Fe_{0.8}O_9$ for the degradation of RhB in the presence of different scavengers (1 mmol L^{-1}) under visible light irradiation.

On the contrary, without the cocatalyst, the photo-generated electron can hardly produce H_2. Hence, the electron is mainly transferred on the RhB, which leads to a relatively large blank (see Fig. 5b). According this opinion, the cocatalyst has more positive influence on the reducing capacity, which decreases the decomposition of RhB. Usually, Au, Ni, Pd, and Pt cocatalysts are good for reduction reactions, such as H_2 production.[18]

4. Conclusions

We prepared $Bi_2Ga_{4-x}Fe_xO_9$ ($0.0 \leq x \leq 1.2$) solid solutions by high-temperature solid-state reaction. Le Bail fitting on powder XRD verified the high purity and crystallinity of the as-prepared samples, and the SEM images show that the $Bi_2Ga_4O_9$ and $Bi_2Ga_{3.2}Fe_{0.8}O_9$ samples are composed of micron and submicron crystallites, respectively. EDS, ICP, and XPS analyses indicated that Fe element is trivalent when incorporated into the $Bi_2Ga_4O_9$ crystal structure. DRS of $Bi_2Ga_4O_9$ and $Bi_2Ga_{3.2}Fe_{0.8}O_9$ samples suggest wide bandgap characteristics and the observed bandgaps are 2.99 eV and 2.59 eV, respectively, assuming the direct semiconductor model. The photocatalytic degradation performance of $Bi_2Ga_4O_9$ was improved by doping Fe^{3+}, adding H_2O_2, and loading a cocatalyst. The optimum photocatalytic performance was obtained using 2.5 wt% $Cu/Bi_2Ga_{3.2}Fe_{0.8}O_9$ sample in the presence of 1.5 mL H_2O_2 under visible light irradiation, whose photo-degradation rate is 8.0 times that of $Bi_2Ga_4O_9$ in the presence of 0.5 mL H_2O_2. This photocatalyst remained stable and active even after four cycles (4 hours in total). The photocatalytic mechanism was suggested as well; the $\cdot OH$ and h^+ played important roles in the photocatalytic degradation reaction.

Conflicts of interest

There are no conflicts to declare.

Acknowledgements

This work was financially supported by the Science and Technology Project of Chongqing Municipal Education Commission (KJQN201801407), Talent Introduction Project of Yangtze Normal University (2017KYQD22).

References

1 W. L. Wang, Y. Z. Cai, H. Y. Hu, J. Chen, J. Wang, G. Xue and Q. Y. Wu, *Chem. Eng. J.*, 2019, **359**, 168–175.
2 J. Y. Liang, X. A. Ning, J. Sun, J. Song, J. Lu, H. L. Cai and Y. X. Hong, *Ecotoxicol. Environ. Saf.*, 2018, **166**, 56–62.
3 M. Ahmad, M. Yousaf, A. Nasir, I. A. Bhatti, A. Mahmood, X. C. Fang, X. Jian, K. Kalantar-Zadeh and N. Mahmood, *Environ. Sci. Technol.*, 2019, **53**, 2161–2170.
4 L. Clarizia, D. Russoa, I. D. Somma, R. Marottaa and R. Andreozzia, *Appl. Catal., B*, 2017, **209**, 358–371.
5 Y. C. Chen, T. C. Liu and Y. J. Hsu, *ACS Appl. Mater. Interfaces*, 2015, **7**(3), 1616–1623.
6 Y. Wu, H. Wang, W. G. Tu, Y. Liu, Y. Z. Tan, X. Z. Yuan and J. W. Chew, *J. Hazard. Mater.*, 2018, **347**, 412–422.
7 W. T. Chen and Y. J. Hsu, *Langmuir*, 2010, **26**(8), 5918–5925.
8 Y. C. Pu, H. Y. Chou, W. S. Kuo, K. H. Wei and Y. J. Hsu, *Appl. Catal., B*, 2017, **204**, 21–32.
9 A. Fujishima and K. Honda, *Nature*, 1972, **238**, 37–38.
10 Y. F. Lin and Y. J. Hsu, *Appl. Catal., B*, 2013, **130–131**, 93–98.
11 Y. C. Pu, W. H. Lin and Y. J. Hsu, *Appl. Catal., B*, 2015, **163**, 343–351.
12 Y. H. Chiu, T. F. M. Chang, C. Y. Chen, M. Sone and Y. J. Hsu, *Catalysts*, 2019, **9**, 430.
13 J. Yang, X. R. Sun, T. Zeng, Y. L. Hu and J. W. Shi, *Materials*, 2019, **12**(9), 1487.
14 J. Yang, H. Fu, D. F. Yang, W. L. Gao, R. H. Cong and T. Yang, *Inorg. Chem.*, 2015, **54**, 2467–2473.
15 Y. H. Chiu and Y. J. Hsu, *Nano Energy*, 2017, **31**, 286–295.
16 M. Y. Chen and Y. J. Hsu, *Nanoscale*, 2013, **5**, 363–368.
17 P. F. Jiang, F. W. Jiang, M. F. Yue, J. Ju, C. L. Xu, R. H. Cong and T. Yang, *Angew. Chem., Int. Ed.*, 2019, **58**(18), 5978–5982.
18 X. B. Chen, S. H. Shen, L. J. Guo and S. S. Mao, *Chem. Rev.*, 2010, **110**, 6503–6570.
19 R. G. Li, F. X. Zhang, D. G. Wang, J. X. Yang, M. R. Li, J. Zhu, X. Zhou, H. X. Han and C. Li, *Nat. Commun.*, 2012, **4**, 1432–1438.
20 Q. X. Jia, A. Iwase and A. Kudo, *Chem. Sci.*, 2014, **5**, 1513–1519.
21 Q. J. Shi, Z. J. Li, L. Chen, X. L. Zhang, W. H. Han, M. Z. Xie, J. L. Yang and L. Q. Jing, *Appl. Catal., B*, 2019, **244**, 541–649.
22 M. B. Tahir, T. Lqbal, H. Kiran and A. Hasan, *Int. J. Energy Res.*, 2019, **43**(6), 2410–2417.
23 H. Sudrajat and S. Hartuti, *Adv. Powder Technol.*, 2019, **30**(5), 983–991.
24 F. Fu, H. D. Shen, X. Sun, W. W. Xue, A. Shineye, J. N. Ma, L. Luo, D. J. Wang, J. G. Wang and J. W. Tang, *Appl. Catal., B*, 2019, **247**, 150–162.
25 X. J. Yuan, D. Y. Shen, Q. Zhang, H. B. Zou, Z. L. Liu and F. Peng, *Chem. Eng. J.*, 2019, **369**, 292–301.
26 Y. D. Hu, G. Chen, C. M. Li, Y. S. Zhou, J. X. Sun, S. Hao and Z. H. Han, *J. Mater. Chem. A*, 2016, **4**(14), 5274–5281.
27 C. H. Lee, H. G. Kim, Y. Gu and D. H. Lim, *Nanosci. Nanotechnol. Lett.*, 2018, **10**, 1179–1186.
28 H. Y. Du and J. F. Luan, *Solid State Sci.*, 2012, **14**(9), 1295–1305.
29 J. Yang, P. F. Jiang, M. F. Yue, D. F. Yang, R. H. Cong, W. L. Gao and T. Yang, *J. Catal.*, 2017, **345**, 236–244.
30 S. X. Ouyang and J. H. Ye, *J. Am. Chem. Soc.*, 2011, **133**, 7757–7763.
31 Z. G. Zou, J. H. Ye, K. Sayama and H. Arakawa, *Nature*, 2001, **414**, 625–627.
32 X. C. Wang, K. Maeda, A. Thomas, K. Takanabe, G. Xin, J. M. Carlsson, K. Domen and M. Antonietti, *Nat. Mater.*, 2009, **8**, 76–80.
33 J. Yang, M. F. Yue, J. Ju, R. H. Cong, W. L. Gao and T. Yang, *Dalton Trans.*, 2014, **43**, 15385–15390.
34 H. X. Yang, B. Q. Shan and L. Zhang, *RSC Adv.*, 2014, **4**, 61226–61231.

35 J. R. Ran, J. Zhang, J. G. Yu, M. Jaroniec and S. Z. Qiao, *Chem. Soc. Rev.*, 2014, **43**, 7787–7812.
36 Z. G. Zou, J. H. Ye and H. Arakawa, *Catal. Lett.*, 2001, **75**, 3–4.
37 J. Singh, S. Sharma, Aanchal and S. Basu, *J. Photochem. Photobiol., A*, 2019, **376**, 32–42.
38 M. Mahanthappa, N. Kottam and S. Yellappa, *Appl. Surf. Sci.*, 2019, **475**, 828–838.
39 L. Zhang, B. Q. Shan, H. X. Yang, D. S. Wu, R. Zhu, J. H. Nie and R. Cao, *RSC Adv.*, 2015, **5**, 23556–23562.
40 R. B. Wei, Z. L. Huang, G. H. Gu, Z. Wang, L. X. Zeng, Y. B. Chen and Z. Q. Liu, *Appl. Catal., B*, 2018, **231**, 101–107.
41 K. Z. Qi, B. Cheng, J. G. Yu and W. K. Ho, *Chin. J. Catal.*, 2017, **38**(12), 1936–1955.
42 Y. C. Chen, Y. C. Pu and Y. J. Hsu, *J. Phys. Chem. C*, 2012, **116**(4), 2967–2975.
43 Y. Y. Shang, X. Chen, W. W. Liu, P. F. Tan, H. Y. Chen, L. D. Wu, C. Ma, X. Xiong and J. Pan, *Appl. Catal., B*, 2017, **204**, 78–88.
44 Z. Wan, G. K. Zhang, X. Y. Wu and S. Yin, *Appl. Catal., B*, 2017, **207**, 17–26.
45 F. Chen, Q. Yang, X. M. Li, G. M. Zeng, D. B. Wang, C. G. Niu, J. W. Zhao, H. X. An, T. Xie and Y. C. Deng, *Appl. Catal., B*, 2017, **200**, 330–342.
46 W. H. Lin, Y. H. Chiu, P. W. Shao and Y. J. Hsu, *ACS Appl. Mater. Interfaces*, 2016, **8**(48), 32754–32763.
47 T. T. Yang, W. T. Chen, Y. J. Hsu, K. H. Wei, T. Y. Lin and T. W. Lin, *J. Phys. Chem. C*, 2010, **114**, 11414–11420.